

Supplement of Biogeosciences, 16, 2923–2936, 2019
<https://doi.org/10.5194/bg-16-2923-2019-supplement>
© Author(s) 2019. This work is distributed under
the Creative Commons Attribution 4.0 License.



Supplement of

Sensitivity of atmospheric CO₂ to regional variability in particulate organic matter remineralization depths

Jamie D. Wilson et al.

Correspondence to: Jamie D. Wilson (jamie.wilson@bristol.ac.uk)

The copyright of individual parts of the supplement might differ from the CC BY 4.0 License.

Supplementary Material

1 Evaluation of the sensitivity analysis approach

Here we provide an evaluation of the approach used to predict atmospheric CO₂ from preformed PO₄ with the Latin hypercube ensemble. A series of sensitivity experiments are performed where the Martin curve exponent in each region is perturbed individually to values of 0.4, 0.7, 1.3, and 1.6 whilst all regions are kept at the control run value of 1.0. All runs are continued from the control run for 3000 years and are run with an explicit carbon cycle. These experiments are used to assess whether disequilibrium of CO₂ air-sea gas exchange (e.g., Eggleston and Galbraith, 2018; Ödalen et al., 2018) violates the statistical relationship between preformed PO₄ and CO₂ (Figure A1) that is used for the Latin hypercube experiments. These experiments are also used to assess whether the regression approach used to define sensitivity (eqn. 2 in the main text) reliably predicts regional patterns of sensitivity.

If disequilibrium of CO₂ air-sea gas exchange is significant when varying Martin curves regionally, the relationship between preformed PO₄ and CO₂ should vary in comparison to when the Martin curve is treated as a globally uniform parameter. The variability between preformed PO₄ and CO₂ from the individual perturbation experiments closely matches variability when the Martin curve is varied globally (Figure S1) suggesting that CO₂ disequilibrium effects are not significant. There are minor deviations suggesting that disequilibrium effects do exist for some regions when varying remineralization depths regionally.

The sensitivity estimates from the Latin hypercube ensemble (Figure 3 in the main text) are compared against the sensitivity of CO₂ from the individual perturbation experiments with the explicit carbon cycle (Figure S2). The sensitivity of CO₂ is calculated in the same way as the Latin hypercube experiments using linear regression (eqn. 2 in the main text). The two estimates agree generally on the relative sensitivity between regions, e.g., there is a correlation coefficient of 0.94 between approaches for both the constant-export and restoring-uptake schemes. There are notable, but minor, differences between the sensitivity approaches. The Latin hypercube estimates are overall slightly lower for both export production schemes (Figures S2a & S2b *cf.* Figures S2c & S2d). Because the Martin curves are varied simultaneously in the Latin hypercube ensemble, this likely reflects that the sensitivity of CO₂ to the Martin curve in one region is offset by concurrent changes in other regions. However, the relative differences are preserved suggesting this is a minor effect. There are also minor changes in the relative sensitivity between regions. For example, the individual perturbation experiments predict that the STemp-IND region is more sensitive than the NN-ATL region for the constant-export model (Figure S2a *cf.* S2c), and that the NTemp-PAC region is less sensitive than the EEq-PAC region in the restoring-uptake model (Figure S2b *cf.* S2d). These differences are within the 95% confidence intervals (Figure 3 in main text) and do not affect the key findings.

2 Evaluation of MITgcm TMM Circulation

2.1 Volumetric Fractions

We compare the volumetric fraction of water sourced from surface regions of the ocean with data-constrained estimates from Khatiwala et al. (2012). The volumetric fraction is obtained by prescribing surface ocean boundary conditions C^B of 1 in the region of interest and 0 elsewhere. The following equation can then be solved to find the interior distribution at steady state:

$$(\mathbf{A}_i^I \mathbf{A}_e^I - \mathbf{I}) \mathbf{C}^I = (\mathbf{A}_i^I \mathbf{B}_e + \mathbf{B}_i) \mathbf{C}^B \quad (\text{S1})$$

The volumetric fraction is then calculated as the volume-weighted mean of the global interior distribution. Table S1 shows the comparison of values from the annual mean MITgcm TMM circulation used in this study and the data-constrained estimates from Khatiwala et al. (2012). Note that there are differences in the exact definition of regions between Khatiwala et al. (2012) and this study.

2.2 Ideal mean age

The ideal mean age (τ_m) shown in Figure S4 is calculated following Khatiwala (2007), where the timestep (dt) is 3.8 days:

$$\tau_m = (\mathbf{A}_i^I \mathbf{A}_e^I - \mathbf{I})^{-1} \mathbf{A}_i^I dt \quad (\text{S2})$$

2.3 Density

- 5 Density is calculated using the Gibbs-Seawater Oceanographic Toolbox (McDougall and Barker, 2011) using annual mean temperature and salinity derived from the global circulation model (Figure S3).

3 Global Averaging of Martin's b parameter

- Here we describe the calculation of a global mean from samples of spatially variable b . Figure S6 shows that when CO_2 is plotted against the global arithmetic mean b of the Latin hypercube samples, there is a constant offset versus runs where b is varied uniformly. We suggest that this offset is a function of a non-linear relationship between b and the amount of organic carbon reaching the ocean interior. This is demonstrated by expressing b as an e -folding depth (the depth at which the proportion of organic matter that has remineralisation = $\frac{1}{e} \approx 0.63$). This is achieved by rearranging the Martin curve equation:

$$F_z = F_{z_0} \left(\frac{z}{z_0} \right)^{-b} \quad (\text{S3})$$

for depth (z) when $\frac{F_z}{F_{z_0}} = \frac{1}{e}$:

$$15 \quad z = \sqrt[b]{\frac{F_z}{F_{z_0}}} z_0 \quad (\text{S4})$$

- where z_0 is the depth of the euphotic zone (here $z_0=120$ m), F_z is the flux of POC at depth z and F_{z_0} is the flux of POC out of the euphotic zone (z_0). e -folding depths get increasingly deeper with decreasing values of b (Figure S7). For example, a change in b from 1.4 to 1.3 results in a decrease in e -folding depth of 14 m whereas a change in b from 0.4 to 0.3 results in a 1902 m. This follows from the fact that the Martin curve represents the scenario of a fixed remineralisation rate and an increasing sinking rate (Kriest and Oschlies, 2008). Therefore, when averaging spatially variable b values, larger values will have disproportionately more weight in comparison to their impact on ocean biogeochemistry.

- To account for this non-linear effect on biogeochemistry, we alternatively calculate the global mean of each Latin hypercube ensemble experiment when converted to e -folding depths. Because of the non-linear relationship between b and e -folding depths, an arithmetic mean is unsuitable (e.g., Figure S8). Instead, we calculate an area-weighted geometric-weighted mean of e -folding depths and convert this back to a value of b .

- An alternative approach to calculating a global mean is to calculate a set of weights based on e -folding depths. However, the calculation of these weights is not straightforward due to issues such as the complete remineralisation of organic matter reaching the seafloor. Alternatively, a Latin hypercube ensemble could be sampled from a uniform distribution of e -folding depths rather than b and applied with an exponential parameterisation of remineralisation. However, power-law based parameters are commonly used in biogeochemical models (e.g., Hülse et al., 2017) as well as in interpreting observations (Honjo et al., 2008). We note that a number of different mathematical functions, each with different mechanistic interpretations and including a power-law and exponential function, are not statistically distinguishable from each other based on existing observations (Cael and Bisson, 2018).

References

- Cael, B. B. and Bisson, K.: Particle Flux Parameterizations: Quantitative and Mechanistic Similarities and Differences, *Frontiers in Marine Science*, 5, 395, <https://doi.org/10.3389/fmars.2018.00395>, <https://www.frontiersin.org/article/10.3389/fmars.2018.00395>, 2018.
- 5 Eggleston, S. and Galbraith, E. D.: The devil's in the disequilibrium: multi-component analysis of dissolved carbon and oxygen changes under a broad range of forcings in a general circulation model, *Biogeosciences*, 15, 3761–3777, <https://doi.org/10.5194/bg-15-3761-2018>, <https://www.biogeosciences.net/15/3761/2018/>, 2018.
- Honjo, S., Manganini, S. J., Krishfield, R. A., and Francois, R.: Particulate organic carbon fluxes to the ocean interior and factors controlling the biological pump: A synthesis of global sediment trap programs since 1983, *Progress in Oceanography*, 76, 217–285, <https://doi.org/10.1016/j.pocean.2007.11.003>, 2008.
- 10 Hülse, D., Arndt, S., Wilson, J. D., Munhoven, G., and Ridgwell, A.: Understanding the causes and consequences of past marine carbon cycling variability through models, *Earth-Science Reviews*, 171, 349 – 382, <https://doi.org/https://doi.org/10.1016/j.earscirev.2017.06.004>, <http://www.sciencedirect.com/science/article/pii/S0012825216303191>, 2017.
- Khatiwala, S.: A computational framework for simulation of biogeochemical tracers in the ocean, *Global Biogeochemical Cycles*, 21, GB3001, <https://doi.org/10.1029/2007GB002923>, <http://dx.doi.org/10.1029/2007GB002923>, 2007.
- 15 Khatiwala, S., Primeau, F., and Holze, M.: Ventilation of the deep ocean constrained with tracer observations and implications for radiocarbon estimates of ideal mean age, *Earth and Planetary Science Letters*, 325-326, 116 – 125, <https://doi.org/doi:10.1016/j.epsl.2012.01.038>, <http://www.sciencedirect.com/science/article/pii/S0012821X12000672>, 2012.
- Kriest, I. and Oschlies, A.: On the treatment of particulate organic matter sinking in large-scale models of marine biogeochemical cycles, *Biogeosciences*, 5, 55–72, <https://doi.org/10.5194/bg-5-55-2008>, <http://www.biogeosciences.net/5/55/2008/>, 2008.
- 20 McDougall, T. J. and Barker, P.: Getting started with TEOS-10 and the Gibbs Seawater (GSW) Oceanographic Toolbox, SCOR/IAPSO WG127, ISBN 978-0-646-55621-5 edn., 2011.
- Ödalen, M., Nycander, J., Oliver, K. I. C., Brodeau, L., and Ridgwell, A.: The influence of the ocean circulation state on ocean carbon storage and CO₂ drawdown potential in an Earth system model, *Biogeosciences*, 15, 1367–1393, <https://doi.org/10.5194/bg-15-1367-2018>, <https://www.biogeosciences.net/15/1367/2018/>, 2018.

Table S1. Global ocean volumetric fraction (%) for different source regions from a data-constrained estimate (Khatiwala et al., 2012) and from this study.

Region	Khatiwala2012 ^a (%)	This Study (%)
Antarctic	39.0	28.7
Subantarctic ^b	18.0	26.1
North Atlantic	26.0	35.0
Tropics ^c	4.5	0.9
Subtropics ^d	8.1	4.5
North Pacific	4.0	4.5

^a Regions defined in Figure 1 of Khatiwala et al., (2012) ^bSubPol-PAC, SubPol-ATL and SubPol-IND regions ^cWEq-PAC, EEq-PAC and Eq-ATL regions ^dSTemp-PAC,NTemp-PAC,STemp-ATL,STemp-ATL,NTemp-PAC and STemp-IND regions

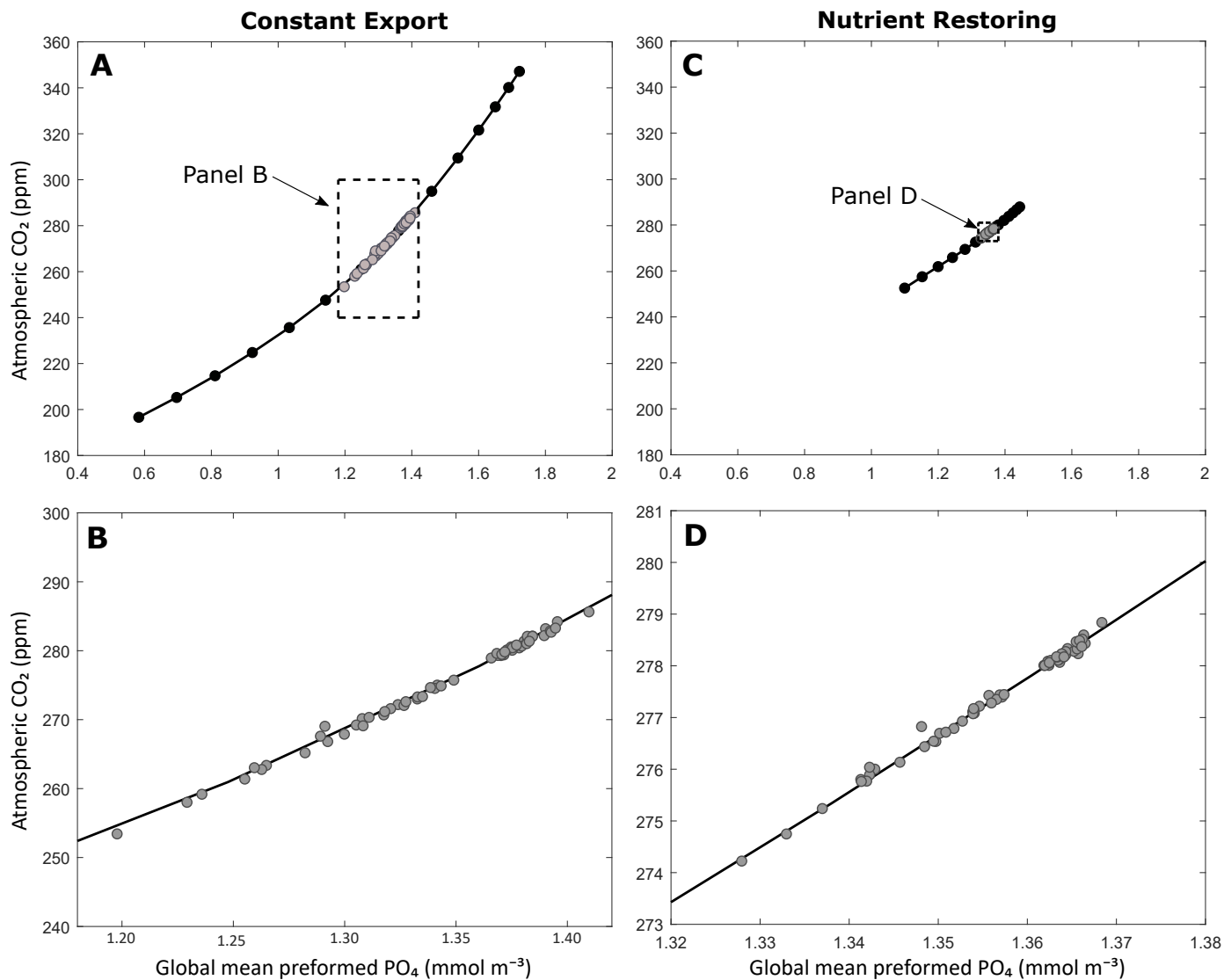


Figure S1. Comparison of CO₂ versus preformed [PO₄] relationships when the Martin curve is varied as a globally uniform value (black line) from -0.4 to -1.6 (see also Figure A1), and when regions are perturbed individually within the same range (grey). Atmospheric CO₂ is explicitly calculated in the model. Panels (a) and (c) show the results for both constant-export and nutrient-restoring ensembles over the full range of preformed PO₄ and CO₂ values (Figure A1). Panels (b) and (d) show the results on expanded axes indicated by the dashed boxes.

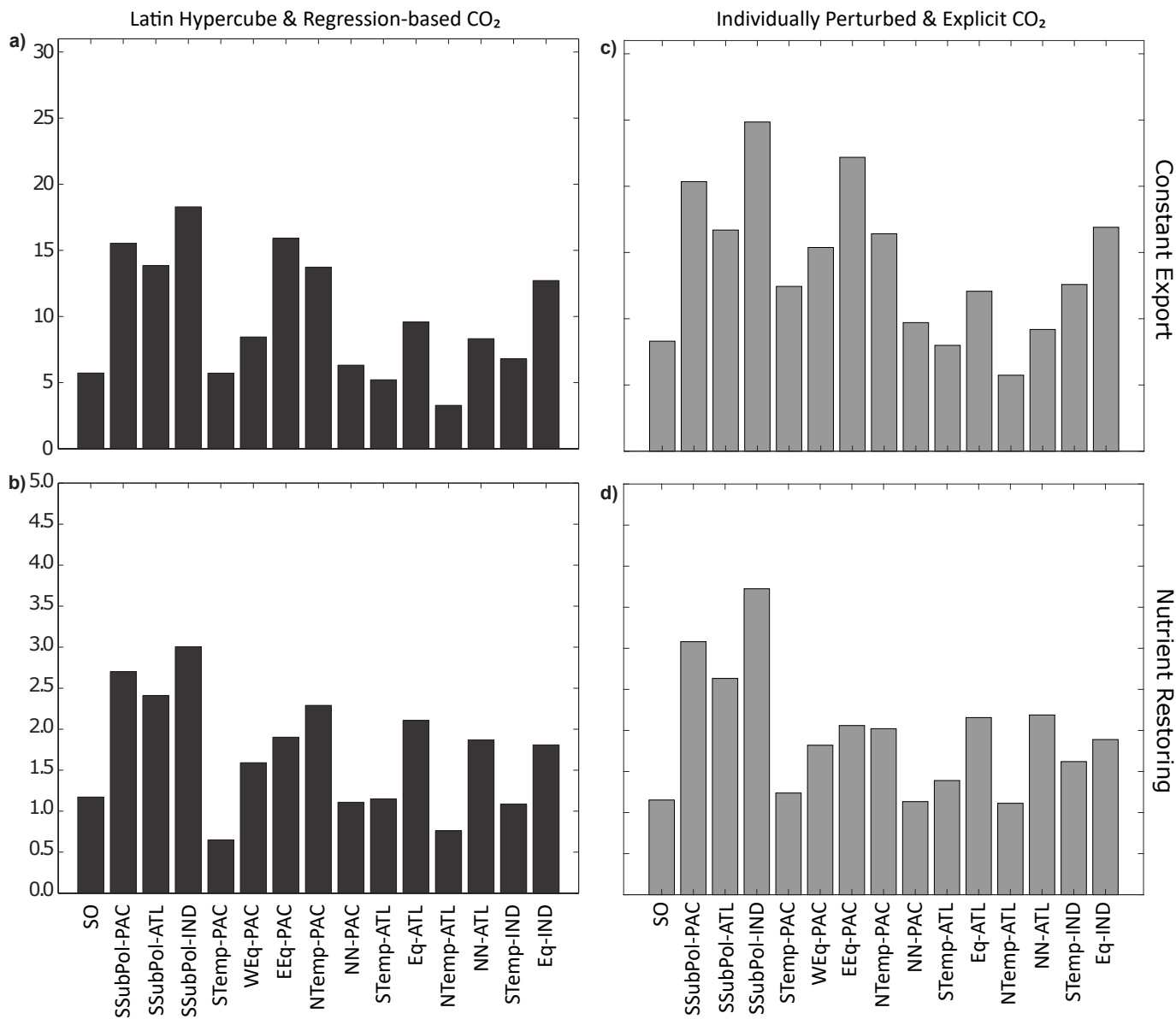


Figure S2. Comparison of CO₂ sensitivity estimates from two methods. Black bars are the Latin hypercube and regression-based sensitivity estimates derived with the statistical relationship preformed PO₄ and CO₂ (Regional Sensitivity experiments described in Section 2.3 of the main text). Grey bars show the sensitivity calculated using the same linear regression approach when each region is perturbed individually from b=0.4 and b=1.6 and atmospheric CO₂ is calculated explicitly in the model as described in Section 1 of the Supplementary material.

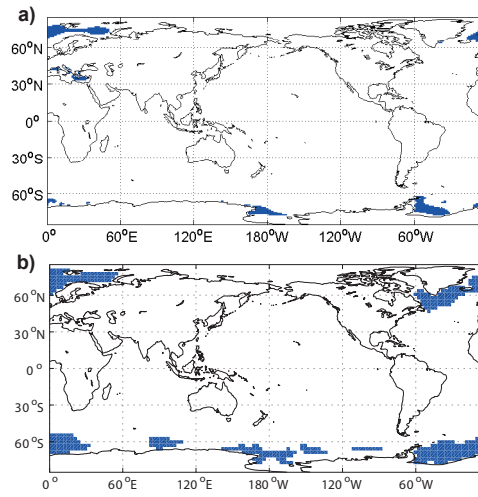


Figure S3. Regions where density is greater than 1027.5 kg m^{-3} calculated using the Gibbs SeaWater toolbox (McDougall and Barker, 2011) with annual-mean temperature and salinity from (a) World Ocean Atlas 18 and (b) MITgcm output.

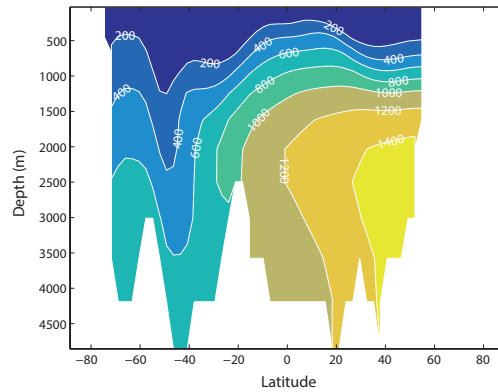


Figure S4. Meridional cross section of ideal age in the Pacific (224°W).

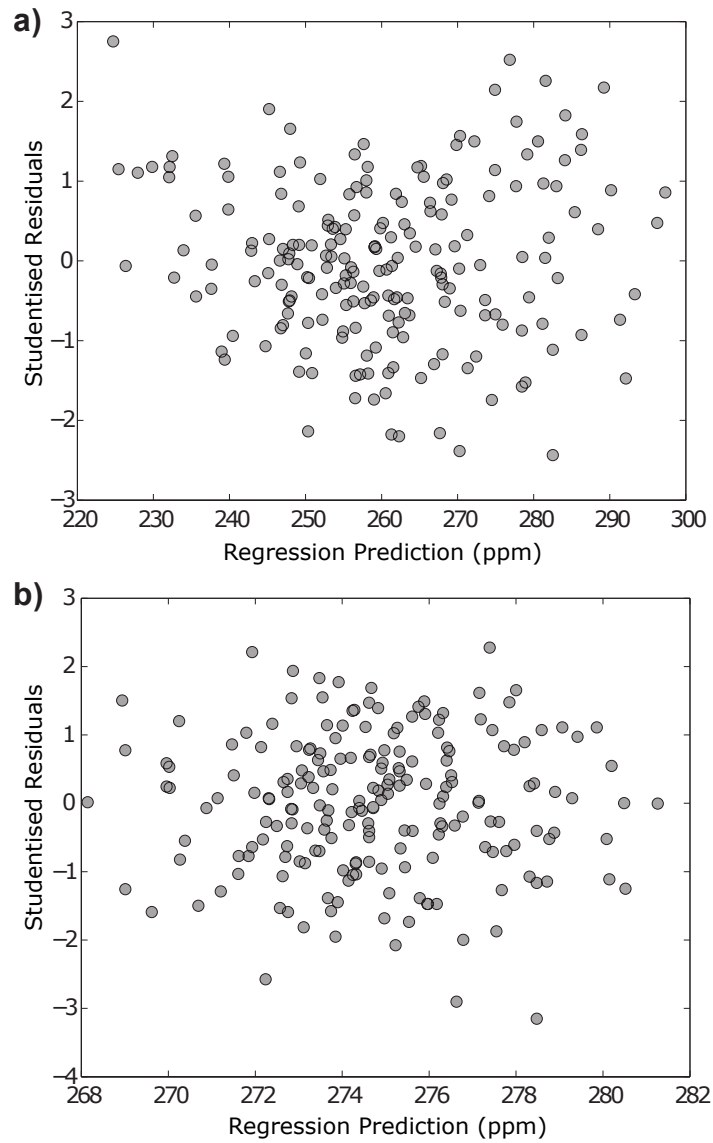


Figure S5. Residuals for the linear regressions (eqn. 2 in the main text) that estimate sensitivity of CO_2 to spatially varying Martin curves for (a) nutrient-restoring and (b) restoring-uptake schemes.

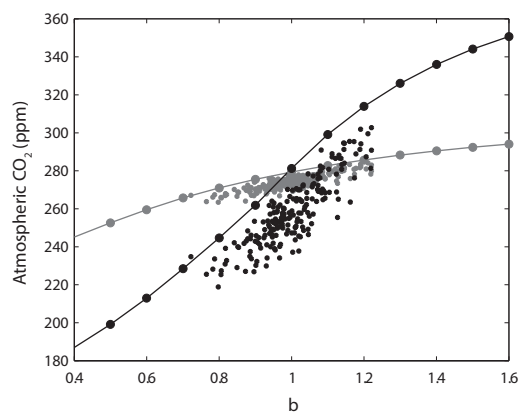


Figure S6. Comparison of CO₂ sensitivity when b is varied as globally uniform parameter (solid lines) and when b is varied regionally in the Latin hypercube samples and calculated as an area-weighted arithmetic mean of b . Runs using the constant-export scheme are shown in black and restoring-uptake runs are shown in grey.

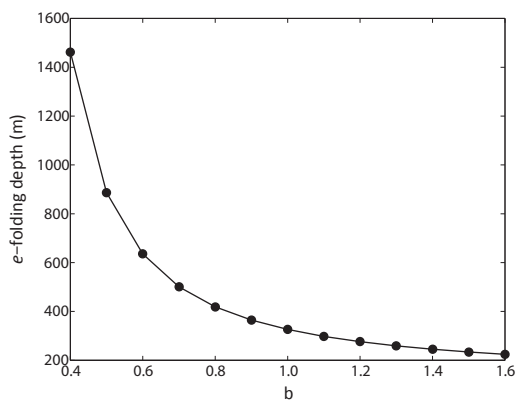


Figure S7. The e -folding depths (depth at which 63% of organic matter has been remineralised) corresponding to various Martin curve exponents. e -folding depths are calculated using eqn. S4.

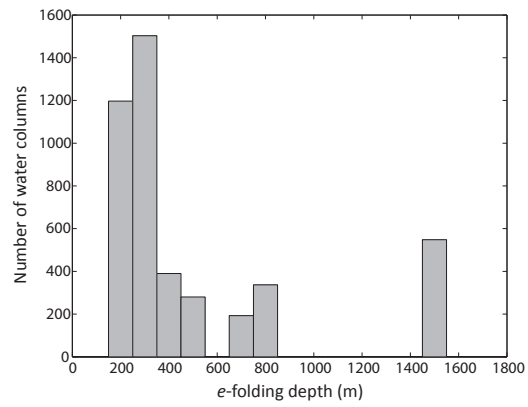


Figure S8. Histogram of e -folding depths for all water columns in the model, calculated from b values from one Latin hypercube sample using equation S4.